



## Conversion of biogas to synthesis gas over NiO/CeO<sub>2</sub>–Sm<sub>2</sub>O<sub>3</sub> catalysts



M. Genoveva Zimicz<sup>a</sup>, Brian A. Reznik<sup>b</sup>, Susana A. Larrondo<sup>c,d,\*</sup>

<sup>a</sup> Instituto de Física del Sur (IFISUR) – CONICET, Av. Alem N°1253, 8000 Bahía Blanca, Buenos Aires, Argentina

<sup>b</sup> Departamento de Ingeniería Química, Facultad de Ingeniería, Universidad de Buenos Aires, Pabellón de Industrias, Ciudad Universitaria, 1428 Buenos Aires, Argentina

<sup>c</sup> División Materiales Funcionales para Celdas de Combustible, CINSO-UNIDEF, Juan B. de La Salle 4397, 1603 Villa Martelli, Buenos Aires, Argentina

<sup>d</sup> Instituto de Investigación e Ingeniería Ambiental, Universidad Nacional de San Martín, UNSAM Campus Miguelete, 25 de Mayo y Francia, 1650 San Martín, Provincia de Buenos Aires, Argentina

### HIGHLIGHTS

- NiO/Ce<sub>0.82</sub>Sm<sub>0.18</sub>O<sub>1.91</sub> cermets were prepared for catalytic and SOFC applications.
- The solids were active without need of pre-treatment.
- The conversion of methane increases with increasing temperature and carbon dioxide to methane molar ratio.
- The catalyst showed a stable behavior during a time on stream of six hours for a carbon dioxide to methane molar ratio of 2.3.

### ARTICLE INFO

#### Article history:

Received 15 March 2014  
Received in revised form 1 September 2014  
Accepted 6 September 2014  
Available online 19 September 2014

#### Keywords:

Biogas  
SOFCs  
Ceria-based materials  
Syngas

### ABSTRACT

The main objective of this work has been to study the catalytic activity in the conversion of biogas to Syngas of a Ni/Ce<sub>0.82</sub>Sm<sub>0.18</sub>O<sub>1.91</sub> oxide system, which could be used as a component in the anode material of a SOFC directly fed with biogas.

The solids were active without need of pretreatment with a stable behavior during a time on stream of six hours for a carbon dioxide to methane molar ratio of 2.3. This feed composition maximize the production of synthesis gas, with stable catalytic behavior without formation of carbonaceous compounds and involving CO<sub>2</sub> capturing, contributing to the reduction of greenhouse gases.

It can be concluded that NiO/CeO<sub>2</sub>Sm<sub>2</sub>O<sub>3</sub> catalysts exhibited promising catalytic performance for their use in the composition of anode material of solid oxide fuel cells fed with biogas.

© 2014 Elsevier Ltd. All rights reserved.

### 1. Introduction

Energy is an integral part of society and plays a vital role in socio-economic development by raising the standard of living. The condition of economic development of a region is directly related to the patterns of consumption and production of energy. In other words, the indexes of energy consumption *per capita* and economic-growth feed each other back and grow together [1].

In recent years, public and political sensitivity regarding environmental care and energy sustainability has led the investigations to the developing of clean and renewable energy sources. Two main concepts have become the guidelines of the development of new technologies for energy supply. These are the utilization of renewable sources of energy and the development of sustainable

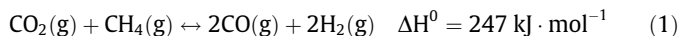
processes. In this context, the biomass arises with a renewed role as a source of renewable fuels, which become an alternative to fossil fuels [2,3]. The main processes of converting biomass into energy include direct combustion, pyrolysis, gasification, liquefaction, anaerobic digestion, alcoholic fermentation and trans-esterification, among others. Each technology has its advantages and disadvantages depending on the type of biomass used [4]. In particular, the conversion of the biogas (mixtures of H<sub>2</sub> and CO) into Syngas constitutes a possible way of revalorization of residential, industrial and agricultural wastes and opens the way for the use of waste for energy production. Syngas has many uses in the industry. It is primarily converted in methanol, which is mainly used in chemical synthesis. Likewise, it can be used as a fuel in solid oxide fuel cells (SOFCs) to provide electrical energy with great efficiency [5,6].

The biogas consists mainly of methane (CH<sub>4</sub>) and carbon dioxide (CO<sub>2</sub>), with some minor components like H<sub>2</sub>S and siloxanes that must be eliminated prior any further transformation process [7]. The direct use of biogas as a fuel in traditional combustion engine

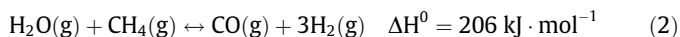
\* Corresponding author at: División Materiales Funcionales para Celdas de Combustible, CINSO-UNIDEF, Juan B. de La Salle 4397, 1603 Villa Martelli, Buenos Aires, Argentina. Tel.: +54 11 47098158.

E-mail address: [susana@di.fcen.uba.ar](mailto:susana@di.fcen.uba.ar) (S.A. Larrondo).

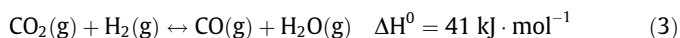
technology to produce heat and electricity is not efficient due to the low calorific power of biogas. The conversion into Syngas through the Dry Reforming of Methane (DRM) emerges as one possibility to take profit of this methane-rich stream. The DRM reaction is a deep endothermic reaction that proceeds according to the following global equation:



This reaction has similarities with the Steam Reforming of Methane (SRM),



However, in the DRM reaction the H to C atomic ratio in the feed stream is lower than in the case of the SRM reaction, creating a higher risk to form carbonaceous deposits. From the thermodynamic analysis presented in the literature it can be seen that these carbonaceous compounds can be formed in a wide range of reaction conditions [8,9]. It can also be concluded from the thermodynamic analysis that the DRM reaction is always accompanied by the Reverse Water Gas Shift reaction (RWGS),



This is the main drawback of the DRM reaction, recently pointed out by Oyama et al. [10], who called attention to the misuse of the DRM reaction for hydrogen production. These researchers noted that this reaction is important for the production of Syngas when it can be directly used without further processing, like in the Gas to Liquid (GTL) processes to obtain liquid fuels, or, as it was mentioned before, as a fuel for SOFCs.  $\text{H}_2$  and CO mixture can be easily electrochemically oxidized in the anode chamber of that kind of fuel cells. In particular, the technology of SOFCs probably constitutes the only technology capable to convert biogas methane directly to syngas taking advantage of the presence  $\text{CO}_2$  in the anode chamber. However, it is necessary to develop appropriate materials for this technology, in particular anode materials having catalytic activity to produce the internal dry reforming of methane and avoiding or disfavoring the formation of carbonaceous residues that would harm the stability of the cell performance [11]. It is important to note that in addition to the catalytic activity of the anode material, this material must have the appropriate ionic and electronic conductivity to allow good performance of the fuel cell.

From the point of view of the catalytic activity, many catalytic systems have been studied for the DRM reaction, showing those based on Rh better performance [1]. However, the developing of Ni-based catalytic systems is important in order to make this technology economically viable in commercial applications. Nickel is an active dehydrogenating catalysts but it is necessary to support it on a system with the capacity to produce the rapid oxidation of the methane dehydrogenated fragments in order to prevent the formation of carbonaceous deposits. Additionally, the support must have basic sites to produce the adsorption of  $\text{CO}_2$ , weakening of the CO–O bond and dissociation or the  $\text{CO}_2$  [3,12]. It is well-known that ceria-based oxides have the capability to easily exchange oxygen with the surrounding atmosphere (Oxygen Storage Capacity, OSC). The partial replacement of  $\text{Ce}^{4+}$  by aliovalent cations, like  $\text{Sm}^{3+}$ , increases the OSC and the number of oxygen vacancies and their mobility, being these vacancies active sites for dissociative adsorption of  $\text{CO}_2$ . Besides, Sm–Ce mixed oxides have emerged as excellent mixed ionic electronic conductors with appropriate properties to be used as electrolytes in SOFCs operating at intermediate temperatures ( $T < 800 \text{ }^\circ\text{C}$ ). Finally, it is important to consider the possibility of the existence of sulfur compounds in the feed. In the literature we can find reports about the sulfur poisoning of Ni-based catalysts during steam reforming

of biogas [13–15]. It was found that the poisoning at low temperature is not recoverable just by removal of  $\text{H}_2\text{S}$  from the feed stream. However, poisoning at high temperature is easily reversed just by removal of  $\text{H}_2\text{S}$  from the feed stream [13]. Moreover, it is well known that ceria-based materials may develop resistance to sulfur poisoning, because the adsorption of sulfur on ceria is reversible for concentration of  $\text{H}_2\text{S}$  below 100 ppm [16].

Based on the information presented in the previous paragraphs, the main objective of this work has been to study the catalytic activity in the conversion of biogas to Syngas of a Ni/Ce<sub>0.82</sub>Sm<sub>0.18</sub>O<sub>1.91</sub> oxide system, which could be used as a component in the anode material of a SOFC directly fed with biogas.

## 2. Materials and methods

The NiO/Ce<sub>0.82</sub>Sm<sub>0.18</sub>O<sub>1.91</sub> catalyst was obtained by the incipient wetness impregnation of ethanolic solutions of Ni(NO<sub>3</sub>)<sub>2</sub> on commercial powders of Ce<sub>0.82</sub>Sm<sub>0.18</sub>O<sub>1.91</sub> (Nextech Materials; specific surface area = 28.6 m<sup>2</sup> g<sup>-1</sup>) in order to get a final content of 9 wt.% of Ni. After the impregnation, the solid is dried at 90 °C and afterwards calcined at 350 °C during two hours, with a heating ramp of 5 °C min<sup>-1</sup>. With this heating treatment all the Ni(NO<sub>3</sub>)<sub>2</sub> is converted to NiO.

The catalysts were characterized with X-ray Powder Diffraction (XPD), Temperature Programmed Reduction (TPR), Scanning Electron Microscopy (SEM) and N<sub>2</sub> physisorption.

XPD experiments were performed with a Phillips PW3710 diffractometer operated with Cu K $\alpha$  radiation and a graphite monochromator. Data was collected in the angular region of  $2\theta = 20\text{--}80^\circ$  with a step size of 0.03° and a time per step of 4 s.

Temperature Programmed Reduction (TPR) experiments were performed in a Micromeritics Chemisorb 2720 equipment using a heating ramp of 10 °C min<sup>-1</sup> in a flow consisting of 5 mol%  $\text{H}_2$  in N<sub>2</sub> (50 cm<sup>3</sup>(STP) min<sup>-1</sup>). The experiments started at room temperature and finished at 920 °C.

The morphology of the samples was examined by SEM technique. The images were obtained with a Zeiss Electron Beam Field Emission SEM-Supra 40. In order to avoid charging problems, the samples were placed over carbon conductive ribbon.

The specific surface area was determined by the BET method from the N<sub>2</sub>-physisorption isotherms obtained at (–196) °C.

Catalytic experiments were performed in a fixed bed lab-scale reactor, operated isothermally and at atmospheric pressure. The reactor consisted of quartz tube of 12 mm outer diameter and 11.2 mm internal diameter. The reactor was placed in an oven provided with a temperature controller. In addition, the catalyst bed was prepared with catalysts and inert material in a mass ratio 1–6 in order to favor temperature uniformity in the catalytic bed. The temperature was monitored with a K-type thermocouple located axially in the center of the catalyst bed, whose signal was transmitted to an electronic thermometer to determine the actual reaction temperature. This thermocouple could be moved along the reactor axe in order to control the isothermicity of the fixed bed. The feed flow was controlled with a mass-flow controller. The compositions of the feed and exit streams were analyzed by on-line gas chromatography using a Clarus 50 Perkin Elmer gas chromatographer equipped with a Thermal Conductivity Detector (TCD) and an automatic injection valve.

Two kinds of catalytic tests were made. The first group of tests studied the evolution of the catalytic performance with temperature: (i)  $Y_{\text{CH}_4}^0 = 0.12$  and molar feed ratio RA ( $Y_{\text{CO}_2}^0/Y_{\text{CH}_4}^0 = 1$ ); (ii)  $Y_{\text{CH}_4}^0 = 0.12$  and molar feed ratio RA in the range 1–2.3; where  $Y_{\text{CH}_4}^0$  and  $Y_{\text{CO}_2}^0$  represent the methane and carbon dioxide molar fraction in the feed.

The second type of test involved the stability study performed at  $Y_{\text{CH}_4}^0 = 0.12$  and molar feed ratio  $RA = 1$ .

Previous catalytic tests were performed in order to assure negligible contribution of the homogeneous reaction, fluid-dynamic behavior compatible with the plug-flow model and chemical control during the catalytic tests [17].

The following expressions will be used to present the catalytic results:

Methane conversion:

$$X_{\text{CH}_4} = \frac{F_{\text{CH}_4}^0 - F_{\text{CH}_4}^s}{F_{\text{CH}_4}^0} \quad (4)$$

where  $F_{\text{CH}_4}^0$  is the methane molar flow in the feed and  $F_{\text{CH}_4}^s$  the methane molar flow in the reactor exit.

Carbon dioxide conversion:

$$X_{\text{CO}_2} = \frac{F_{\text{CO}_2}^0 - F_{\text{CO}_2}^s}{F_{\text{CO}_2}^0} \quad (5)$$

where  $F_{\text{CO}_2}^0$  is the carbon dioxide molar flow in the feed and  $F_{\text{CO}_2}^s$  the carbon dioxide molar flow in the reactor exit.

Hydrogen production:

$$P_{\text{H}_2} = \frac{F_{\text{H}_2}^s}{2 \cdot F_{\text{CH}_4}^0} \quad (6)$$

where  $F_{\text{H}_2}^s$  is the hydrogen molar flow in the reactor exit.

Carbon monoxide production:

$$P_{\text{CO}} = \frac{F_{\text{CO}}^s}{F_{\text{CH}_4}^0 + F_{\text{CO}_2}^0} \quad (7)$$

### 3. Results and discussion

#### 3.1. Characterization of fresh catalyst

In Fig. 1 the XPD patterns of support, nickel oxide and fresh catalyst are plotted together. In the diffraction pattern of the support it is possible to see the typical fluorite structure of the ceria-based materials. The diffraction pattern of the fresh catalyst corresponds to the overlapping of support and nickel oxide diagrams. No additional peaks were observed.

In Fig. 2 the TPR profiles of Ce–Sm support, nickel oxide and NiO/Ce<sub>0.82</sub>Sm<sub>0.18</sub>O<sub>1.91</sub> catalyst are depicted together. Pure NiO

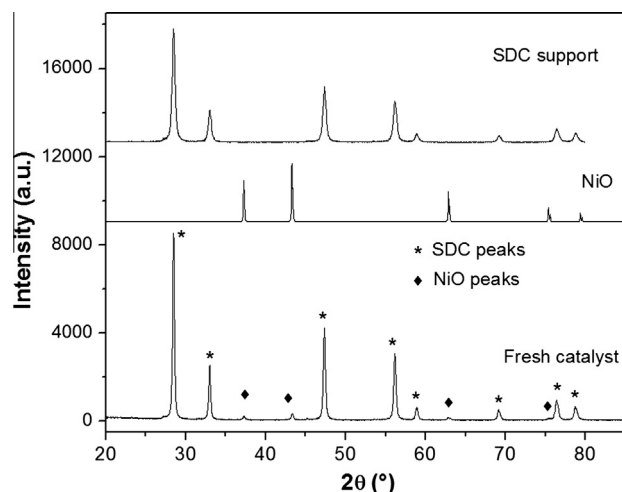


Fig. 1. XPD diffraction pattern of Ce–Sm support, nickel oxide and fresh catalyst.

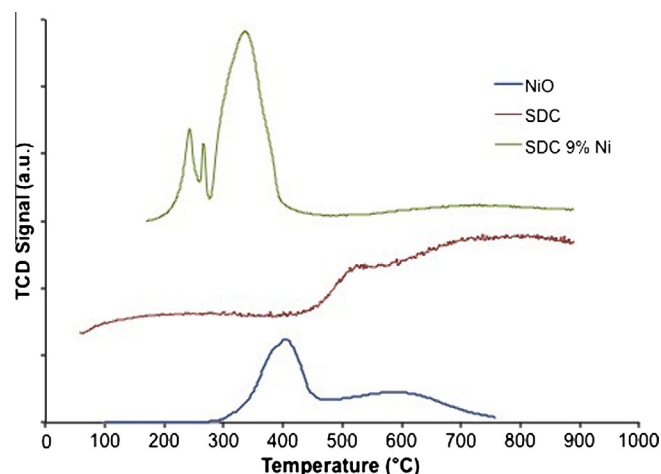
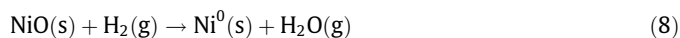


Fig. 2. TPR profiles of NiO, support (SDC) and fresh catalyst (SDC 9% Ni).

profile shows two peaks, the first one at 400 °C and the second one at 570 °C. Quantifying the hydrogen consumption yields to a percentage of reduction of  $100 \pm 5\%$ , pointing out that the oxide reduces according to the following equation:



Analyzing the TPR profile of the Ce–Sm support, it can be seen that the TPR profile shows a shoulder at the temperature of 500 °C and a very broad peak at 800 °C. Quantifying the hydrogen consumption, it is obtained a total reduction of 31% of the cerium sites present in the solid. This is consistent with the fact that the replacement of Ce<sup>4+</sup> cations by Sm<sup>3+</sup> leads to the formation of oxygen vacancies and stabilizes the oxidized state of cerium cations.

The NiO/Ce<sub>0.82</sub>Sm<sub>0.18</sub>O<sub>1.91</sub> TPR profile is complex and cannot be obtained as a superposition of the profiles of the NiO and the Ce–Sm support, indicating a synergistic effect between the support and the supported phase. It can be observed a broad reduction profile with a wide reduction temperature range: 170–900 °C, with two unresolved peaks in the 200–300 °C region, with maxima at 235 °C and 275 °C, a very intense peak at 350 °C and a broad peak at 730 °C. The reductions of both NiO and Ce–Sm support have moved to lower temperatures. The NiO is more easily reduced when supported while the main reduction peak of the support remains broad but with the maximum slightly shifted to lower temperatures. It is widely considered that low temperature peaks are related to relatively free NiO species, while high temperature peaks are associated to NiO species that strongly interact with the support. This strong interaction enhances ceria reducibility, most probably due to enhancement of oxygen mobility in the Ce–Sm support [18,19].

A SEM micrograph image of the fresh catalyst is shown in Fig. 3. Two different particle sizes can be observed, one about 30 nm in size which corresponds to the support and the larger one about 70 nm in size corresponding to NiO. The mapping results obtained by Electron Diffraction Spectroscopy (EDS) are also presented in Fig. 3 indicating a good distribution of nickel on the surface. Atomic percentage values of metal cations determined by EDS in three different points of the sample are consistent with the nominal values.

The BET specific surface area of the catalyst was obtained from the N<sub>2</sub> physisorption isotherm. Five points were considered in the isothermal region corresponding to relative pressure below 0.3. A specific surface area of 26 m<sup>2</sup> g<sup>−1</sup> was obtained. Comparing with the value corresponding to the support, it is clear that a reduction of a 10.5% in the specific surface area was produced in the impregnation and calcination performed to support the NiO phase.

### 3.2. Catalytic tests

In Fig. 4 methane and carbon dioxide conversions are plotted as a function of reaction temperature for stoichiometric composition in the feed ( $RA = 1$ ), space-time of  $28.8 \text{ g h dm}^{-3}$ (CNPT), and  $Y_{\text{CH}_4}^0 = 0.12$ . The conversion of methane and carbon dioxide increases with increasing temperature. It is important to note that carbon dioxide conversion is always higher than the methane conversion at temperatures below  $800 \text{ }^\circ\text{C}$ . This fact is usually attributed to the occurrence of the RWGS reaction, in which carbon dioxide reacts with the hydrogen produced to generate water and carbon monoxide. It is important to note, that in the reactor exit there is a silica-gel fixed bed to trap any trace of water produced during the process, in order to avoid its entrance to the gas chromatographer. At higher temperatures the conversions tend to be equal. In Fig. 5 the production of hydrogen and carbon monoxide are depicted together. It is noted that at low temperatures, yields have a similar value. At temperatures above  $700 \text{ }^\circ\text{C}$  the  $\text{H}_2$

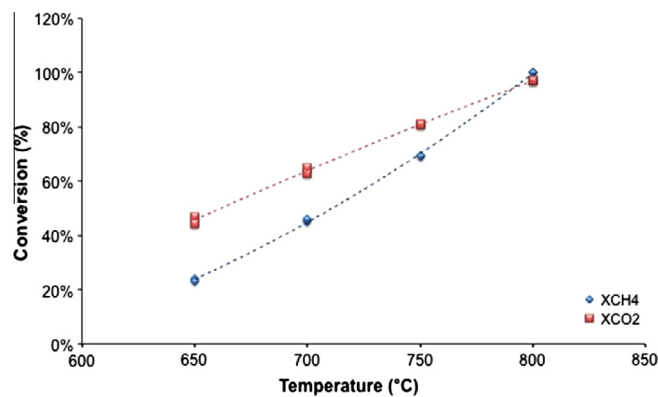


Fig. 4.  $\text{CH}_4$  and  $\text{CO}_2$  conversion vs. temperature;  $RA = 1$ ; space-time =  $28.8 \text{ g h dm}^{-3}$ (CNPT).  $Y_{\text{CH}_4}^0 = 0.12$ .

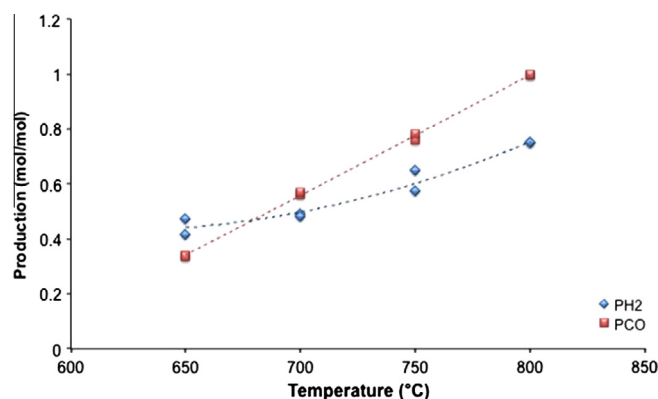


Fig. 5. Hydrogen and carbon monoxide production vs. temperature;  $RA = 1$ ; space-time =  $28.8 \text{ g h dm}^{-3}$ (CNPT).  $Y_{\text{CH}_4}^0 = 0.12$ .

production is slightly lower than that of CO production. These results cannot be explained only with the occurrence of DRM and RWGS reactions. In order to see whether carbon deposits have been formed during the experiments, stability studies were performed. In Fig. 6 the evolution of methane and carbon dioxide conversions with time on stream are presented. The conversion of methane is very stable during the test period. However, the carbon dioxide conversion slightly decreases with time on stream,

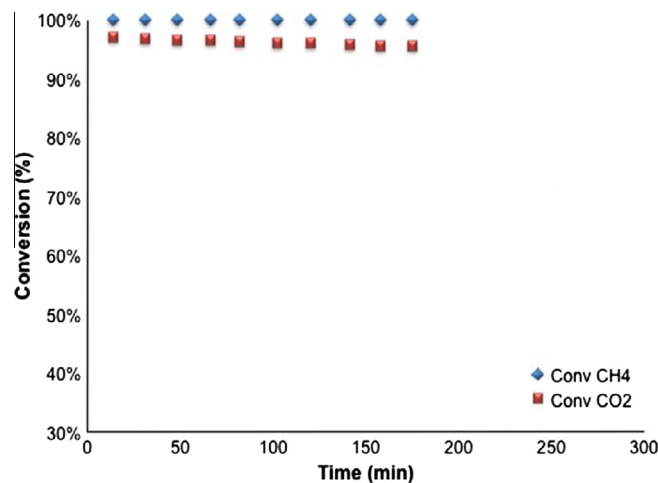
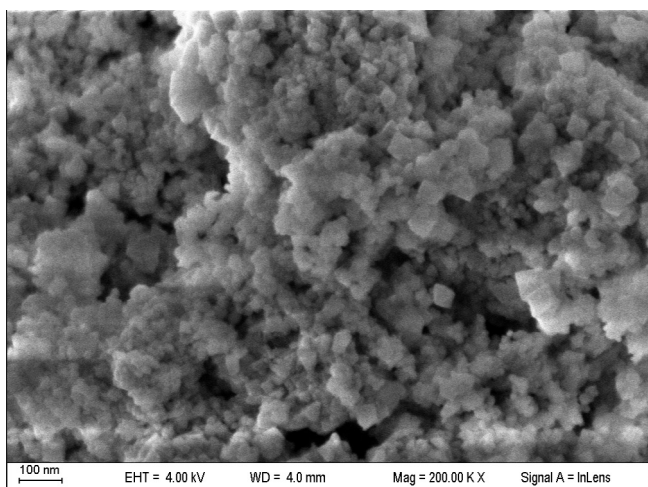
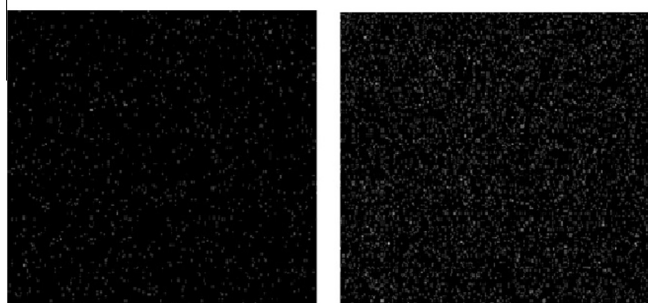


Fig. 6.  $\text{CH}_4$  and  $\text{CO}_2$  conversions vs. time on stream during stability tests;  $RA = 1$ ; space-time =  $28.8 \text{ g h dm}^{-3}$ (CNPT).  $Y_{\text{CH}_4}^0 = 0.12$ .

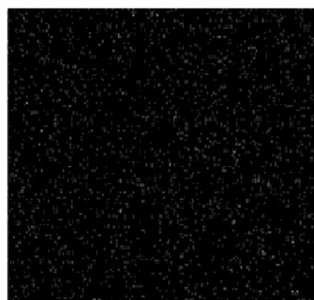


(a)



Ni Ka1

Ce La1



Sm La1

(b)

Fig. 3. (a) SEM micrograph image of fresh catalyst; (b) EDS mapping of cations.

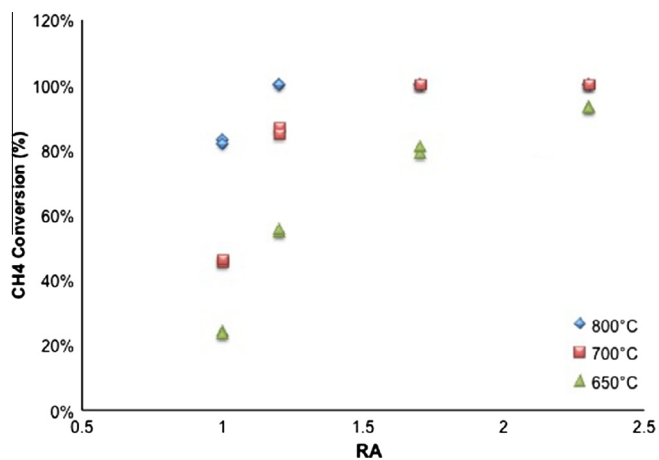


Fig. 7. CH<sub>4</sub> conversions vs. RA; space-time = 28.8 g h dm<sup>-3</sup>(CNPT). Y<sub>CH<sub>4</sub></sub><sup>0</sup> = 0.12.

indicating a deactivation process probably occurring by the deposition of carbonaceous deposits over the support. XPD pattern of spent catalysts confirmed the presence of the more intense peak of graphite. Besides, the more intense peaks corresponding to Ni<sup>0</sup> were also detected, indicating that NiO reduces during the experiments.

Catalytic studies for different feed ratios, in the range 1–2.3, were performed. RA values below 1 were not tested since they favor carbon deposition. In Fig. 7 it is possible to observe that methane conversion increases with increments in the feed ratio, reaching 100% for RA = 2.3 for all the temperatures. Stability tests were performed with this feed ratio observing a stable behavior over 6 h on stream. Besides, the XRD patterns of the spent catalysts showed no peaks corresponding to carbon.

#### 4. Conclusions

Regarding the synthesis of the catalyst it was observed that the NiO was in a separate phase with a uniform distribution over the support surface. The solids were active without need of pre-treatment. The conversion of methane increases with increasing temperature and carbon dioxide to methane molar ratio. The catalyst showed a stable behavior during a time on stream of six hours for a carbon dioxide to methane molar ratio of 2.3.

It can be concluded that NiO/CeO<sub>2</sub>–Sm<sub>2</sub>O<sub>3</sub> catalysts exhibited promising catalytic performance for their use in the composition of anode material of solid oxide fuel cells fed with biogas. Furthermore, the conditions that maximize the production of synthesis gas, with stable catalytic behavior without formation of carbonaceous compounds involves capturing CO<sub>2</sub>, contributing to the reduction of greenhouse gases.

#### Acknowledgements

The post-doctoral scholarship granted to M. Genoveva Zimic by the CONICET is gratefully acknowledged. This research received financial support from PIDDEF 011/11 MINDEF and Premio FOCA 2013, Banco Galicia.

#### References

- [1] Katuwal H, Bohara AK. Biogas: a promising renewable technology and its impact on rural households in Nepal. *Renew Sust Energ Rev* 2009;13:2668–74.
- [2] Munster M, Lund H. Optimal use of organic waste in future energy systems – the danish case. *Riso Int Energy Conf* 2007.
- [3] Dodić SN, Popov SD, Dodić JM, Ranković JA, Zaravago ZZ, Glousin MT. An overview of biomass energy utilization in Vojvodina. *Renew Sust Energ Rev* 2010;14:550–3.
- [4] Bridgewater AV, Toft AJ, Brammer JG. A techno-economic comparison of power production by biomass fast pyrolysis with gasification and combustion. *Renew Sust Energ Rev* 2002;6:181–246.
- [5] Vayenas CG, Bebelis SI. In: Gellings PJ, Bouwmeester HJM, editors. *The CRC handbook of solid state electrochemistry*. London: CRC Press; 1997 [chapter 13].
- [6] Van Herle J, Membrez Y, Bucheli O. Biogas as a fuel source for SOFC co-generators. *J Power Sources* 2004;127:300–12.
- [7] Plou J, Durán P, Herguido J, Peña JA. Purified hydrogen from synthetic biogas by joint methane dry reforming and steam-iron process: behaviour of metallic oxides and coke formation. *Fuel* 2014;118:100–6.
- [8] Edwards JH, Maitra AM. The chemistry of methane reforming with carbon dioxide and its current and potential applications. *Fuel Process Technol* 1995;42:269–89.
- [9] Nikoo MK, Amin NAS. Thermodynamic analysis of carbon dioxide reforming of methane in view of solid carbon formation. *Fuel Process Technol* 2011;92:678–91.
- [10] Oyama ST, Hacarlioglu P, Gu Y, Lee D. Dry reforming of methane has no future for hydrogen production: comparison with steam reforming at high pressure in standard and membrane reactors. *Int J Hydrogen Energy* 2012;37(13):10444–50.
- [11] Van Herle J, Membrez Y, Bucheli O. Biogas as a fuel source for SOFC co-generators. *J Power Sources* 2004;127:300–12.
- [12] Flores E, Fuentealba P, Mondragon F. Chemical reactivity of oxygen vacancies on the MgO surface: reactions with CO<sub>2</sub>, NO<sub>2</sub> and metals. *Catal Today* 2008;133–135:216–22.
- [13] Appari S, Janardhanan VM, Bauri R, Jayanti S. Deactivation and regeneration of Ni catalyst during steam reforming of model biogas: an experimental investigation. *Int J Hydrogen Energy* 2014;39:297–304.
- [14] Appari S, Janardhanan VM, Bauri R, Jayanti S, Olaf Deutschmann D. A detailed kinetic model for biogas steam reforming on Ni and catalyst deactivation due to sulfur poisoning. *Appl Catal A* 2014;471:118–25.
- [15] Ashrafi M, Christoph Pfeifer, Tobias Pröll, Hofbauer H. Experimental study of model biogas catalytic steam reforming: 2. Impact of sulfur on the deactivation and regeneration of Ni-based catalysts. *Energy Fuels* 2008;22:4190–5.
- [16] Yun JW, Yoon SP, Park S, Kim HS, Nam SW. Analysis of the regenerative H<sub>2</sub>S poisoning mechanism in Ce<sub>0.8</sub>Sm<sub>0.2</sub>O<sub>2</sub>-coated Ni/YSZ anodes for intermediate temperature solid oxide fuel cells. *Int J Hydrogen Energy* 2011;36:787–96.
- [17] Perego C. Experimental methods in catalytic kinetics. *Catal Today* 1999;52:133–45.
- [18] Roh HS, Jun KW, Dong WS, Chang JS, Park SE, Joe YI. Highly active and stable Ni/Ce–ZrO<sub>2</sub> catalyst for H<sub>2</sub> production from methane. *J Mol Catal A* 2012;181:137–42.
- [19] Pengpanich S, Meeyoo V, Rirksomboon T. Methane partial oxidation over Ni/CeO<sub>2</sub>–ZrO<sub>2</sub> mixed oxide solid solution catalysts. *Catal Today* 2004;93–95:95–105.